Journal of Energy Storage 163 (2026) 122209

Contents lists available at ScienceDirect

Journal of Energy Storage

journal homepage: www.elsevier.com/locate/est

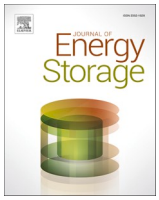

Research papers

The impact of convexity and concavity in modeled core-shell electrode pores on faradic and EDL capacitances: A comparison across spherical geometries

Ezat Keshavarzi *, Fatemeh Dehghan Safiabad, Samaneh Safdaar

Department of Chemistry, Isfahan University of Technology, 8415683111, Isfahan, Iran

ARTICLE INFO

Keywords:
Pseudo-capacitor
Core-shell model
Potential drop in the stern region
Electrochemical reaction
EDL thickness

ABSTRACT

The impact of different spherical geometry of electrode pores, core, core-shell, shell, beside of yolk-shell on the Faradic and EDL capacitances were investigated by combining electrochemical reactions with Modified Fundamental Measure Theory. The behaviors of the capacitance with concentration, pore size, electrode potential, and wall curvature have been studied and explained via potential drop in the stern region and EDL thickness. The two bird and bell shapes of the total capacitance curves have been observed due to the different concentration. Our results show that the core-shell model, with both convex and concave surfaces, is a unique spherical geometry for increasing capacitance. This observation may be explained via the confinement effect and the greater electric field. Our findings demonstrate that at low potential, as well as high potentials when the pore thickness is larger than 2 times the ion's diameter the larger capacitance is mainly related to field strength. To separate the effect of concave and convex walls in Faradic capacitance, the results for core-shell geometry have been compared with two other spherical geometries, a core one with a convex wall and a shell type model with a concave surface which our results show that the core-shell model is superior in comparison to both of them in increasing the capacitance.

1. Introduction

Supercapacitors, as electrochemical energy storage devices, are optimal for applications requiring rapid response and great power density [1]. It is well known that two types of mechanisms are expected for energy storage in supercapacitors; non-Faradic processes based on electrostatic adsorption, which are named electric double-layer capacitors (EDLc) and Faradic process known as pseudo-capacitors which acts based on the reversible electrochemical reaction [2]. The Faradic and electric double-layer (EDL) capacitances play different roles in electrochemical energy-storage systems. The EDL capacitance, which originates from the rapid adsorption of ions at the electrode surface, is well suited for high-power and fast-response uses, including power buffering and short-term load leveling. In contrast, the Faradic capacitance, arising from reversible redox reactions, provides higher energy density and therefore becomes more important in applications that require larger amounts of stored energy [3–5]. Therefore, understanding and controlling the balance and distribution of these two components through pore geometry design, material selection, and electrolyte conditions enables the rational design of electrodes that simultaneously optimize both power and energy. Such insights can be applied to the design and optimization of asymmetric supercapacitors, flashes deliver power, portable and wearable electronics, energy recovery systems, as well as ionic separation processes [5].

It's important to introducing the supercapacitors with high capacitance, energy density without sacrificing the power density and cycle life [6]. Achieving optimal performance in supercapacitors requires the development of specific combinations of electrodes, electrolytes, separators, and current collectors. Among of the mentioned parameters which contribute to the performance of the supercapacitor, the electrolytes and electrode materials have the most significant impact on the operating potential window and therefore the capacitance.

From microscopic point of view the capacitance is predominantly influenced by the thickness and charge of EDL beside of the surface properties of porous electrodes. In fact, the porosity, shape, size, and morphology of the electrode have an important role in the performance of the supercapacitor [7]. When the pore size is comparable to the electrolyte ions' size, it maximizes the utilization of pore space and

* Corresponding author.
E-mail address: keshavrz@iut.ac.ir (E. Keshavarzi).

https://doi.org/10.1016/j.est.2026.122209
Received 25 March 2025; Received in revised form 4 December 2025; Accepted 8 April 2026

achieves optimal capacitance [8,9]. As we know the transport of ions in nanoscale systems differs from those ones in bulk electrolytes due to the confinement of electrolytes into the pores. This confinement has also an impact also on electrochemical reaction. Largeot et al. investigated the impact of nanopore size on the capacitance of an electric double layer supercapacitor. They found that pores that are very close to the size of electrolyte ions have the highest capacitance additionally, both larger and smaller pores showed a reduction in capacitance [10]. It should be noted that the EDL overlaps in the EDL structure for small pores, due to limited space for screening the surface potential, has significant in the amount of energy storage [11,12]. Jiménez et al. illustrated that at low surface potentials, when ions are subjected to severe confinement conditions, approximately at 2 nm or less (only slightly larger than the size of hydrated ions), EDL overlap is observed. Under these conditions, the concentrations of counterions, surface charge density, and EDL capacitance are all relatively small. Additionally, the findings of their study indicate that EDL overlap does not occur in micropores under conditions of low surface potentials combined with high ionic strength or at large surface potentials [12]. Beside of the role of the surface area of electrodes and its pore size, the pore geometry is an important factor that significantly effects on the ion adsorption at the interface of the electrode-electrolyte [13,14]. Many theoretical studies have been focused on examining the capacitance of porous electrodes with different pore geometries, such as slit, cylinder, and spheres. Theoretical results indicate that supercapacitor charging behavior is significantly influenced by the convexity, or concavity, of nanoscale surfaces [15]. For surfaces with the same convex curvature, the contact density and zeta potential are lower than those on the flat surfaces. In contrast, for surfaces with concave curvature, the order is reversed: flat surfaces are associated with lower values, followed by cylindrical surfaces, and spherical surfaces have the highest values [15–18]. The potential applied to the electrode surface dictates which the convex or concave surface contributes to the rise in capacitance [19]. Reindl et al. investigated the curvature effect on the capacitance of electrolytes in contact with planar, spherical, and cylindrical electrodes. Their findings revealed that the capacitance is notably impacted by the surface charge density in the case of electrodes with small curvatures, while the influence of surface charge on electrodes with larger curvatures is negligible [20].

Also, modification of the electrode surface by doping heteroatoms such as nitrogen, oxygen, boron, and/or sulfur onto the porous surface can affect o both electric double-layer capacitance and pseudo-capacitance, leading to improved performance in supercapacitors [14,21,22].

The oxygen functional groups on the carbon electrode can be categorized as acidic or basic. Acidic groups include hydroxyl, carboxyl, and phenol, while basic groups include ketone, quinone, and carbonyl. It is easy for basic groups to pick up protons in acidic environments, and acidic groups combine with hydroxyl ions in an alkaline solution (OH) [23,24]. Su at el. used classical density functional theory to show how a simple molecular model can describe the electric double layer when there are Faradic reactions. They showed that adding oxygen functional groups to planar electrodes raises the Faradic capacitance but doesn't have much effect on the electrical double layer capacitance. Theoretical predictions correspond with the experimental observations [25].

The main goals of this article, is investigated the impact of various of spherical geometries and pore size on EDL structure and Faradic capacitance by using a powerful technique, namely the combination of surface electrochemical reaction and classical density functional theory (CDFT).

It should be noticed that different spherical have been synthesized in experiments. Among yolk-shell structures, metal oxide hollow structures, and hollow carbon nanomaterials, are in attention due to their features such as void space, large surface area, effective light absorption, and resistance to volumetric expansion [26–28]. Although these structures offer many advantages, challenges such as precise control over features like shell thickness, core diameter, and particle size remain [29]. Through modeling these structures, we can gain a deeper understanding of their behavior and performance, enabling the development of improved synthetic methods and optimized applications in energy storage and conversion systems. To this end in this article, we have considered a core-shell model for the pores of electrodes and investigated the effect of both concave and convex walls of the pores simultaneously on the Faradic and EDL capacitance. A key innovation of this research to the consideration of functional groups and the application of electric potential to both surfaces, concave and convex ones, in the case of core-shell model, and investigated Faradic and EDL capacitance. Also, examined the role of the potential drop in the Stern region in the amount of capacitance. We have also studied the impact of different spherical geometries on Faradic capacitance for three different structures: spherical core-shell pores, spherical shells, and spherical cores. Finally, we investigate the effects of the electric field and confinement effects by comparing three spherical pore models, including core-shell, yolk-shell, and shell pores.

2. Model and method

2.1. Modeling of the faradic reaction at the electrode surface

The system being studied consists of porous electrodes that are immersed in acidic solution which contains ions of the same size. Fig. 1 depicts the porous electrodes of a pseudo-capacitor with core-shell spherical pores. These pores are made up of two homo-center spheres, an aspherical core with a radius of R_{in}, which is inside a larger sphere or spherical shell with a radius of R_{out}. Note that ions are distributed between two homocentric spheres in these pores, and are in equilibrium with bulk electrolyte. On the other words, the ions have been confined between two concave and convex walls of the pore related to the shell and core respectively. This type of pore has been chosen because it is possible to investigate the effect of both concave and convex walls of the pore on the capacitance behavior.

Considering the basic oxygenated functional groups (B) on the convex and concave surfaces of these pores, the Faradic reaction is possible, which enhances the supercapacitor's capacitance. The Faradic reaction of the basic groups on the surface in the presence of an acidic solution can be represented by the following equation:

$$B + \mathrm{H}^+ + e^- \leftrightarrows P \quad K = \frac{a_P}{a_{\mathrm{H}^+} a_B} = \frac{N\theta}{N(1-\theta)\, a_{\mathrm{H}^+}}$$

$$N(1-\theta) \qquad\qquad N\theta \tag{1}$$

where B, is a functional group on the surface of the electrode, that exists in its oxidized state, and as a result of the reaction, P is produced in its reduced state. N is used to denote the site densities of basic functional groups on the electrode surface. θ represents the fraction of active sites that interact with H^+ ions under any applied potential.

As a first approximation in the Eq. (1), the activities of functional groups (a_P and a_B) has been presented by site densities. The amount of charge density storage on the electrode as a result of the Faradic reaction [25], Q_F, may be obtained as;

$$Q_F = -eN\theta \tag{2}$$

where θ is;

$$\theta = \frac{K a_{\mathrm{H}^+}}{K a_{\mathrm{H}^+} + 1} \tag{3}$$

The activity of H^+, a_{H^+}, is equal to γ_i [H^+], where the activity coefficient, γ_i, may be obtained via CDFT. In fact, we used the Modified Fundamental Measure Theory (MFMT) in the framework of the restricted primitive model (RPM) to obtain a_{H^+}, which in the next section we present a brief review on it. The activity coefficient may be expressed within the RPM as follows;

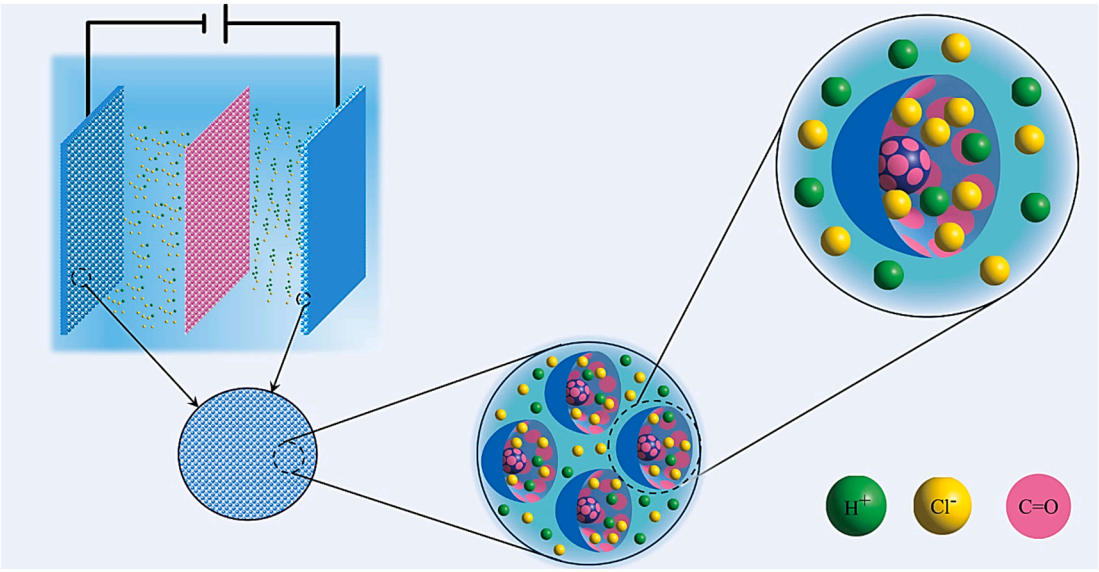

Fig. 1. Schematic representation of the microscopic structure of the electrode for pseudo-capacitor with a core-shell pores, basic oxygenated functional groups on it has been also shown.

$$k_B T \ln\gamma_i = \mu_{i,ex} = \mu_{i,ex}^{hs} + \mu_{i,ex}^{el} + Z_i e \Psi(r) \tag{4}$$

where $\mu_{i,ex}^{hs}$ and $\mu_{i,ex}^{el}$ are the local excess chemical potential due to hard-sphere repulsion and electrostatic correlation, Z_i and e are the valence ions and the unit charge respectively. $\Psi(r)$ also is the mean electrostatic potential (MEP).

Finally, by determining Q_F using Eq. (2), the integral of Faradic capacitance, C_F, is;

$$C_F = \left|\frac{Q_F}{\Psi(R)}\right| = \left|-eN\frac{\theta}{\Psi(R)}\right| \tag{5}$$

where $\Psi(R)$ is the electrode potential. To get the total Faradic capacitance of a core-shell spherical pore, we should calculate the capacitance related to the core part, $C_{F,in}$ and the shell ones $C_{F,out}$ in parallel manner, resulting:

$$C_F = \frac{C_{F,in}{R_{in}}^2 + C_{F,out}{R_{out}}^2}{\left({R_{in}}^2 + {R_{out}}^2\right)} \tag{6}$$

Besides the Faradic reaction, the formation of the EDL at the interface of the electrode-electrolyte can cause the storage of the charge on the electrode. The amount of net ion charges into the core-shell pores can be obtained via density distributions of ions, $\rho_i(r)$, by the following equation:

$$Q_{ion} = \frac{q_{ion}}{4\pi\left({R_{in}}^2 + {R_{out}}^2\right)} = \frac{4\pi\sum_{i=a,b} z_i e \int_{R_{in}}^{R_{out}} r^2 \rho_i(r) dr}{4\pi\left({R_{in}}^2 + {R_{out}}^2\right)} \tag{7}$$

Therefore, the integral capacitance of the electric double-layer supercapacitor (C_{EDL}) is;

$$C_{EDL} = \left|\frac{Q_{ion}}{\Psi(R)}\right| \tag{8}$$

The Faradic and EDL capacitances are combined in a parallel manner, therefore the total capacitance, C_{Total}, is determined by

$$C_{Total} = C_F + C_{EDL} \tag{9}$$

2.2. Classical density functional theory

For the system of interest, the electrolyte into the pore is in equilibrium with the bulk electrolyte, at a constant temperature, T, volume, V, and chemical potential, μ_i. In this condition, the thermodynamic potential function of the system is the grand potential. Grand potential function is obtained by Legendre transformation of Helmholtz free energy with respect to N_i variables, as follows:

$$\Omega[\{\rho_i\}] = F[\{\rho_i\}] - \sum_{i=a,b} N_i \mu_i \tag{10}$$

In the given equation, $\{\rho_i\}$ represents the density distribution of each species. The symbol μ_i represents the chemical potential, and $F[\{\rho_i\}]$ stands for the Helmholtz free energy function. In our studied system the two ions, a and b, have been modeled as charged hard spheres, and therefore $F[\{\rho_i\}]$ includes the following terms:

$$F[\{\rho_i\}] = F^{id}[\{\rho_i\}] + F_{ex}^{hs}[\{\rho_i\}] + F_{ex}^{c}[\{\rho_i\}] + F_{ex}^{el}[\{\rho_i\}] + F_{ext}[\{\rho_i\}] \tag{11}$$

$F^{id}[\{\rho_i\}]$ is the ideal contribution, $F_{ex}^{hs}[\{\rho_i\}]$ is the hard sphere contribution [30,31], $F_{ex}^{c}[\{\rho_i\}]$ is the direct Coulombic contribution [32], $F_{ex}^{el}[\{\rho_i\}]$ is the electrostatic correlation contribution [18], and $F^{ext}[\{\rho_i\}]$ is the contribution of the external field on the ions. The calculation of each of these terms for the studied system is given in our previous work [33]. The chemical potential of ions can be calculated using the expression for their bulk one as;

$$\mu_i = \mu_i^{id} + \mu_{i,ex}^{hs} + \mu_{i,ex}^{c} + \mu_{i,ex}^{el} \tag{12}$$

where $\mu_{i,b}^{id}$ and $\mu_{i,b,ex}^{hs}$ are the contributions related to the ideal and the hard sphere where the latter can be determined using the Boublik–Mansoori–Carnahan–Starling–Leland (BMCSL) equation for the bulk [34], $\mu_{i,b,ex}^{c}$ is the chemical potential due to Coulomb interactions, and $\mu_{i,b,ex,}^{el}$ represent the contributions of electrostatic correlation. To obtain the ion's densities distributions, we minimize $\Omega[\{\rho_i\}]$ with respect to the ion's densities as follow;

$$\left(\frac{\partial\Omega[\{\rho_i\}]}{\partial\rho_i(r)}\right)_{T,V,\mu} = \left(\frac{\partial F^{id}}{\partial\rho_i(r)} + \frac{\partial F_{ex}^{hs}}{\partial\rho_i(r)} + \frac{\partial F_{ex}^{c}}{\partial\rho_i(r)} + \frac{\partial F_{ex}^{el}}{\partial\rho_i(r)} + V_{ext}(r) - \mu_i\right) = 0 \tag{13}$$

By inserting the derivations related to the different contributions of the Helmholtz free energy into Eq. (13), the Euler-Lagrange equation is obtained as follows:

$$\rho_i(\mathbf{r}) = \rho_i^b exp\left[-\beta\left(\frac{\partial F_{ex}^{hs}}{\partial \rho_i(\mathbf{r})}\right)_{T,V,\mu} + \sum_{i=1}^{N} \times \int \Delta C_{ij}^{(2)el}(|\mathbf{r}' - \mathbf{r}|) \times \left[\rho_i(r') - \rho_i^b\right] d\mathbf{r}' - \beta Z_i e\left[\Psi(\mathbf{r}) - \Psi^b\right] + \beta\mu_{i,hs}^{ex}\right)\right] \quad (14)$$

$\Delta C_{ij}^{(2)el}$ is the excess electrostatic direct correlation function, which has been reported in Ref [35]. The Euler-Lagrange equation, $\Psi(r)$, is related to the sum of the two terms of $\frac{\partial F_{ex}^{c}}{\partial \rho_i(\mathbf{r})}$ and $V^{ext}(\mathbf{r})$ as follows [36]:

$$Z_i e\Psi(\mathbf{r}) = \frac{\partial F_{ex}^{c}}{\partial \rho_i(\mathbf{r})} + V^{ext}(r) \quad (15)$$

Also $\Psi(\mathbf{r})$ can be obtained by solving Poisson's equation, using the two following boundary conditions as;

$$\begin{cases} \left(\frac{d\Psi(r)}{dr}\right)_{r=R_{in}} = -\frac{Q_{R_{in}}}{\varepsilon} \\ \Psi_{r=R_{out}} = \Psi(R_{out}) \end{cases} \quad (16)$$

where $Q_{R_{in}}$ equal to $\frac{q_{in}}{4\pi R_{in}^2}$ which q_{in} is the amount of charge on the core, convex surface, The solvent has been considered a continuum medium with a relative dielectric constant, $\varepsilon_r = \frac{\varepsilon}{4\pi\varepsilon_0}$, equal to 78.5. The result of the Poisson's equation for spherical core-shell pore is;

$$\Psi(r) = \Psi(R_{out}) - \frac{1}{\varepsilon}\left(\frac{q_{in}}{R_{out}}\right) + \frac{1}{\varepsilon}\left(\frac{q_{in}}{r}\right) - \sum_i \frac{4\pi}{\varepsilon(R_{out})} z_i e \times \int_{R_{in}}^{R_{out}} r^2\rho_i(r)dr + \sum_i \frac{4\pi}{\varepsilon r_1} z_i e \int_{R_{in}}^{r_1} r^2\rho_i(r)dr + \sum_i \frac{4\pi}{\varepsilon} z_i e \int_{r_1}^{R_{out}} r\rho_i(r)dr \quad (17)$$

where "r" represents an arbitrary point within the core-shell pore, which it gets different values between R_{in} to R_{out}. We have also imposed the condition of equality of $\Psi(R)$ on both concave and convex surfaces as;

$$\Psi(R_{in}) = \Psi(R_{out}) = \Psi(R) \quad (18)$$

To satisfy this condition the following equation (Eq. (19)) should be also valid for the equilibrium densities in addition to Euler-Lagrange equation (Eq. (14)).

$$-\frac{1}{\varepsilon}\left(\frac{q_{in}}{R_{out}}\right) + \frac{1}{\varepsilon}\left(\frac{q_{in}}{R_{in}}\right) = \sum_i \frac{4\pi}{\varepsilon(R_{out})} z_i e \int_{R_{in}}^{R_{out}} r^2\rho_i(r)dr - \sum_i \frac{4\pi}{\varepsilon} z_i e \times \int_{R_{in}}^{R_{out}} r\rho_i(r)dr \quad (19)$$

It should be noted that in order to solve the Euler-Lagrange equation, the input data, besides the temperature, the electrolyte concentration, $\Psi(R_{out})$, the sizes of the pore and the ions, is an initial guess for q_{in}, q_{in}^g, according to Eq. (17) to calculate $\Psi(r)$. The Euler-Lagrange equation (Eq. (14)) has been solved via the iterative method. The iteration continues until the difference between two consecutive density distributions for each of the ions at each point is less than 10^{-4}. These densities can be considered as the equilibrium densities, if they also satisfy Eq. (17). In fact, in this way the value of $\Psi(R_{in})$ is equal to $\Psi(R_{out})$, means the initial guess for q_{in}^g is correct. Otherwise, we repeat our calculations with another guess for q_{in}^g. These calculations repeat until the equilibrium densities satisfy Eq. (19) in addition to the Euler-Lagrange equation. Finally, the average density of H^+, $\overline{\rho}_{H^+}$, may be obtained by its local equilibrium density distribution as;

$$\overline{\rho}_{H^+} = \frac{4\pi}{\frac{4}{3}\pi\left[(R_{out}^*)^3 - (R_{in}^*)^3\right]} \int_{R_{in}^*}^{R_{out}^*} \rho_{H^+}^*(r) r^{*2} dr^* \quad (20)$$

The concentration of H^+ may be obtained by $\overline{[H^+]} = \frac{\overline{\rho}_{H^+}}{1000 \times N_A \times \sigma^3}$, where N_A and σ are Avogadro's number and ions diameter. Fig. 2 illustrates the flowchart of the programming presented, where the results of CDFT are combined with surface electrochemical reactions to determine the Faradic capacitance.

The validity of the model and programming was checked previously [37] with a Monte Carlo simulation inside the core-shell pore. The reported result shows excellent agreement between the two approaches.

3. Results and discussion

3.1. The faradic and EDL capacitance curves

As we know the Faradic capacitance is influenced by various parameters, including electrolyte concentration, size of the pores, and applied potential. As a first try we investigate the effect of electrolyte concentration on Faradic reaction, for simplicity we have considered a

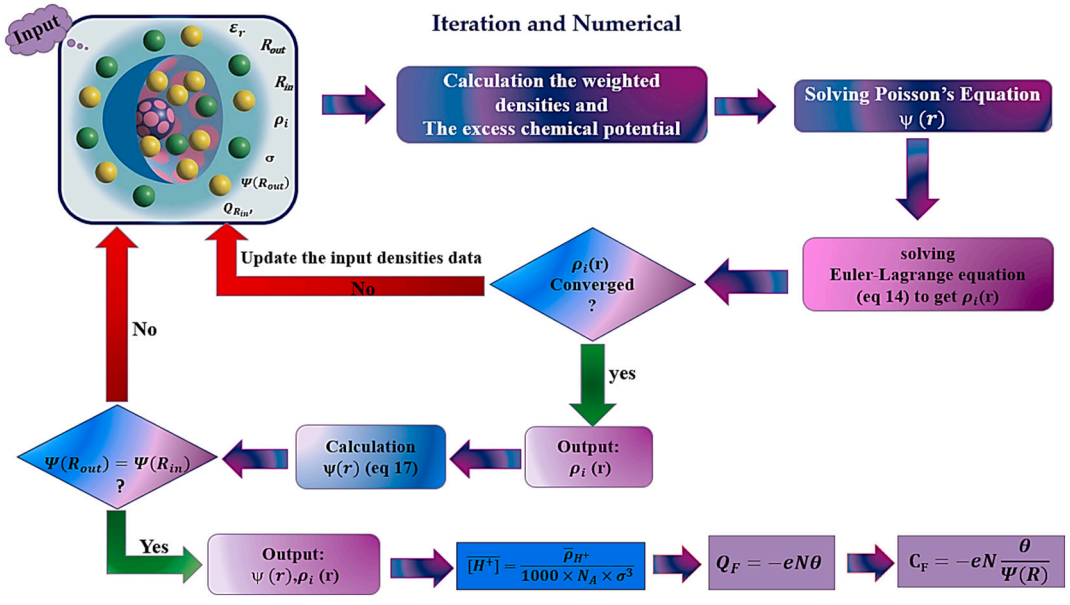

Fig. 2. A flowchart detailing our calculation method for determining Faradic capacitance.

single core-shell spherical pore with a size of $R_{in} = 2\sigma$ and $R_{out} = 3.5\sigma$ where the number densities of oxygenated group, N_{Total}, on it is equal to 0.1 nm^{-2}. We have also assumed that the equilibrium constant for the Faradic reaction is equal to unity, $K = 1$. It is important to note that changing the equilibrium constant affects the capacitance values, but the overall trend and also our discussion remains unchanged.

Fig. 3a. shows the fraction of active sites, which interact with H^+, θ, as a function of potential for different (+1: −1) electrolyte concentrations including 0.5, 1.0, 1.5 and 2.0 M at a temperature of 298 K. For simplicity and consistency with our theoretical framework, we assume that both cations and anions in aqueous solutions are fully hydrated, modeled as charged hard spheres with an effective diameter of 0.5 nm, in line with previous studies [25].

Fig. 3b depicts the average density of H^+, $\overline{\rho}_{H^+}$, which adsorbed into the pore versus $\Psi(R)$ under conditions similar to those ones in Fig. 3a. According to Eqs. (2) and (3), it is clear that the average concentration of H^+, $[H^+]$, into the pore has a close relation with the behavior of θ versus $\Psi(R)$. As one can see when the negative potential on the electrode surface increases $\overline{\rho}_{H^+}$ increases, for all examined concentration which enhances the functional group reactivity. As the number of sites involved in the reaction is limited, all functional groups are involved in the reaction and θ goes to unity at a specific potential depending on concentration. It means increasing the potential to higher value will not have an impact on the reactivity and therefore the charge storage via the Faradic mechanism.

At positive potential, the concentration of H^+ into the pore decreases and goes to zero due to electrostatic repulsion with the pore walls. Therefore, no significant reaction can occur. Also, Fig. 3a shows that θ curve shifts towards positive potentials with concentration. This means that at high concentrations, the adsorption of H^+ occurs even at low positive potentials. On the other words, the range of the potential at which the electrochemical reactions can occur, increases with concentration.

Fig. 4a shows the Faradic capacitance curve, calculated from Eq. (5), at the same condition of Fig. 3a. As we expected the Faradic reaction mainly occurs at the low negative potential approximately at $\Psi(R) = -0.01$ V. According to Fig. 4a, the supercapacitor's Faradic capacitance increases with concentration, resulting in more charge storage. In summary, increase in the concentration of H^+ in the bulk causes an increase $\overline{\rho}_{H^+}$ into the pore, leading to an expected increase in the Faradic capacitance due to the more electrochemical reaction.

Fig. 4b illustrates the integral EDL capacitance curve at the same conditions depicted in Fig. 4a. The symmetric shape of capacitance curve is due to the equal size and valance of the cations and anions. As shown in the figure, the capacitance curve can be either camel-shaped at low concentration or bell-shaped (at higher concentration). In fact, depending on the electrolyte concentration, a transition from camel-shaped to bell-shaped one can occur. For the camel curve of the EDL capacitance, a minimum observed near zero potential where the two maximums appear at higher positive and negative potentials respectively. (see the curve related to the concentrations of C = 0.5 M and 1.0 M). The minimum and maximum of the camel curves are associated with the formation of a wide diffuse and the compact layers of ions into the pore. In fact, at low concentrations, the compact layer of ions is not formed at nearly zero potential. However, at higher concentrations, the compact layer can be formed easily around zero potential. In summary, we may say that as the electrolyte concentration increases, the gap between the two maximums in the camel capacities curve decreases till they coincide to each other at nearly zero potential. Leads to bell curve capacitance (see the graph related to 1.5 and 2.0 M concentrations).

The total capacitance curve for a core-shell pore, according to Eq. (9), which is the sum of EDL and Faradic capacitance has been also shown for different concentrations, including 0.5, 1.0, 1.5 and 2.0 M in Fig. 4c. As one can see, at low electrolyte concentrations, the combination of Faradic and EDL capacitance results a bird-shaped curve. On the other words, the appeared peak at nearly zero potential related to Faradic capacitance while the two others are related to the EDL one. Additionally, the capacitance curve related to 1.5 and 2.0 M have a bell shape because both of the maxima related to Faradic and EDL capacitance have been appeared at nearly zero potential. In fact, the transitions from a bird-shaped capacitance to a bell one corresponds to the concentration for which the EDL capacitance has a bell shape.

3.2. *Effect of pore size on faradic and EDL capacitance*

Fig. 5a shows $\overline{\rho}_{H^+}$ inside pores with different sizes in contact of an acidic electrolyte solution with a concentration of 1.0 M. In this figure, the value of R_{in} has been fixed at 2σ, while the R_{out} has different values, including 3.5, 4, 5, and 6.5σ. In fact, by increasing R_{out}, the pores' thickness, $H = R_{\text{out}} - R_{\text{in}}$, increases. As one can see, at negative potentials, $\overline{\rho}_{H^+}$ decreases with size. Our results show that although the number of H^+ increases with size, its increase compared to the increase in the volume of the pore is less, leading to a reduction in the average density of H^+ ions into the pore.

Fig. 5b shows the functional groups' reactivity at the pore surface at the same conditions as Fig. 5a. As one can see at positive potential branch by increasing the thickness of the pore the reactivity decreases and it goes to zero at higher potentials. This may be explained by the fact that with an increase in the thickness of the pore, a larger number of H^+ ions are adsorbed, and therefore a higher positive potential is required for their desorption. In fact, we have an electrochemical reaction until H^+ is despaired totally from the pore. However, in the negative branch

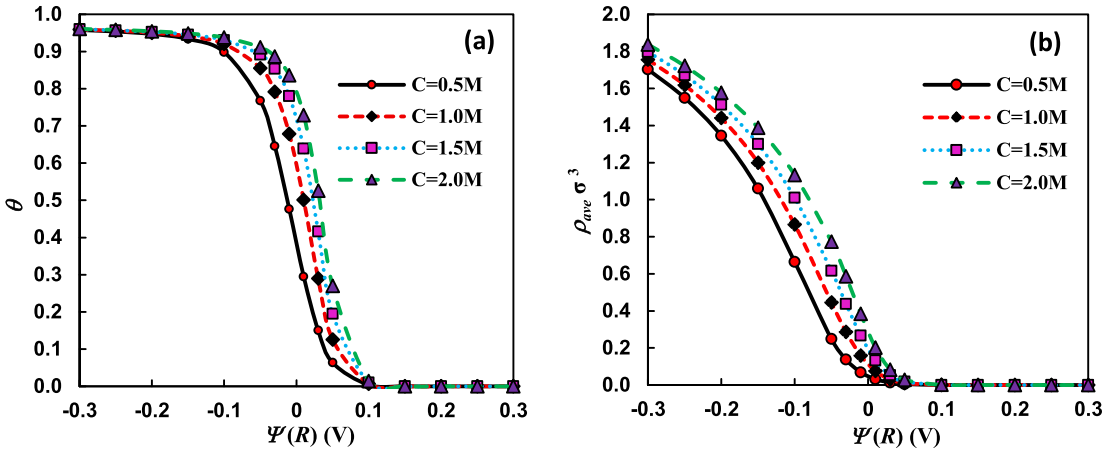

Fig. 3. ***a*** θ versus $\Psi(R)$ related to the of core-shell spherical pore with a size of $R_{\text{in}} = 2\sigma$ and $R_{\text{out}} = 3.5\sigma$ and ***b*** the average density of H^+ $\Psi(R)$ for different concentrations, including 0.5, 1.0, and 2.0 M.

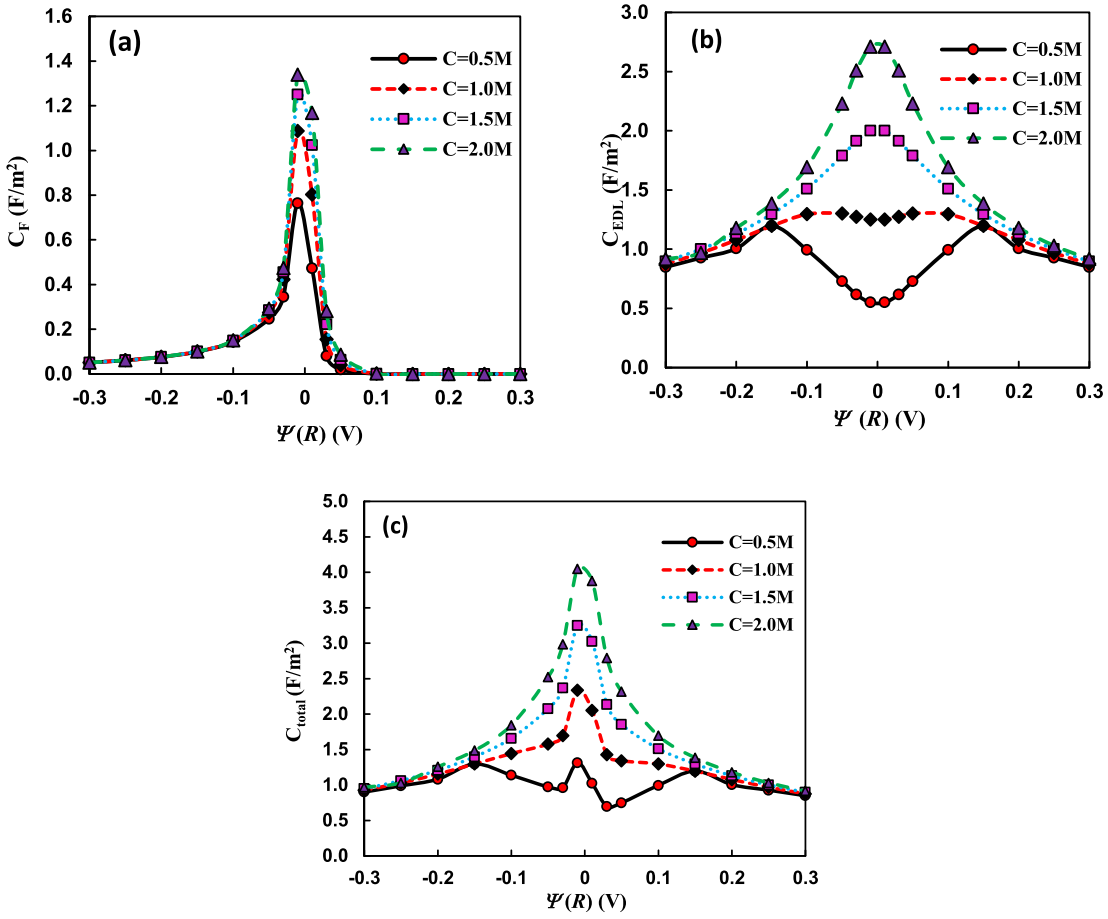

Fig. 4. The integral Faradic capacitance ***a***, The EDL ***b*** and the total capacitance ***c*** curve for core-shell spherical pore with a size of Rin = 2σ and Rout = 3.5σ the other conditions are the same as Fig. 3a.

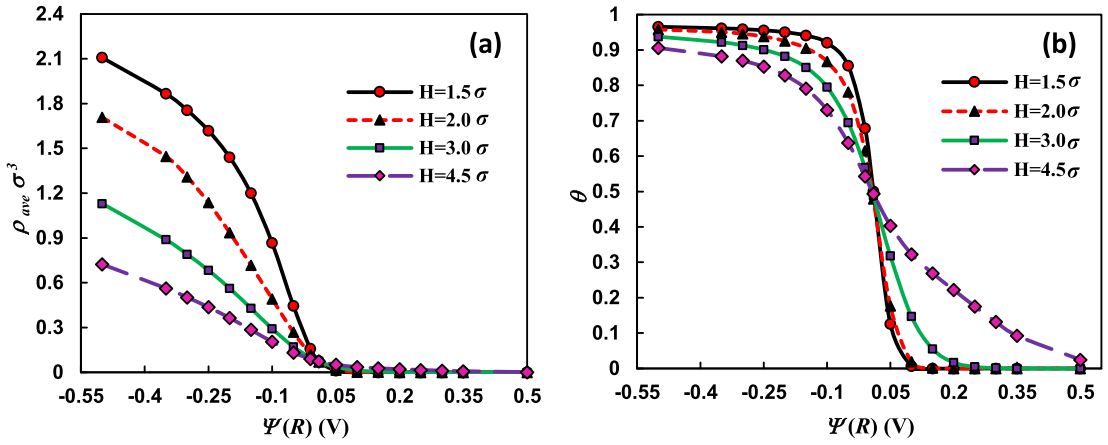

Fig. 5. ***a*** The average density of H^+ and ***b*** the fraction of active sites involved in the reaction as a function of potential for core-shell spherical pore where R_{in} is constant at 2σ, while R_{out} varies, including 3.5, 4, 5, and 6.5σ at electrolyte concentrations of equal to 1.0 M.

of the potential, it goes to unity at lower potential for smaller pores. This can be explained by formation of the more compact layer of H^+ ion into the smaller pore due to the confinement effect.

In Fig. 6a, the integral Faradic capacitance for various pore sizes for the core-shell model has been shown at the same condition related to as Fig. 5a.

As we expected at positive potential branch, the Faradic capacitance is greater for larger thicknesses. Conversely, at negative potentials, the Faradic capacitance decreases with size. The maximum Faradic capacitance is observed at an applied potential nearly equal to $\Psi(R) = -0.01$ V. The inset plot in Fig. 6a, enlarged the behavior of the Faradic capacitance around a potential equal to −0.01 V. According to this figure is the maximum value of Faradic capacitance decreases with pore size. This decrease is attributed to the decreases in the average density of H^+ with size.

Fig. 6b shows the integral EDL capacitance curve at the same

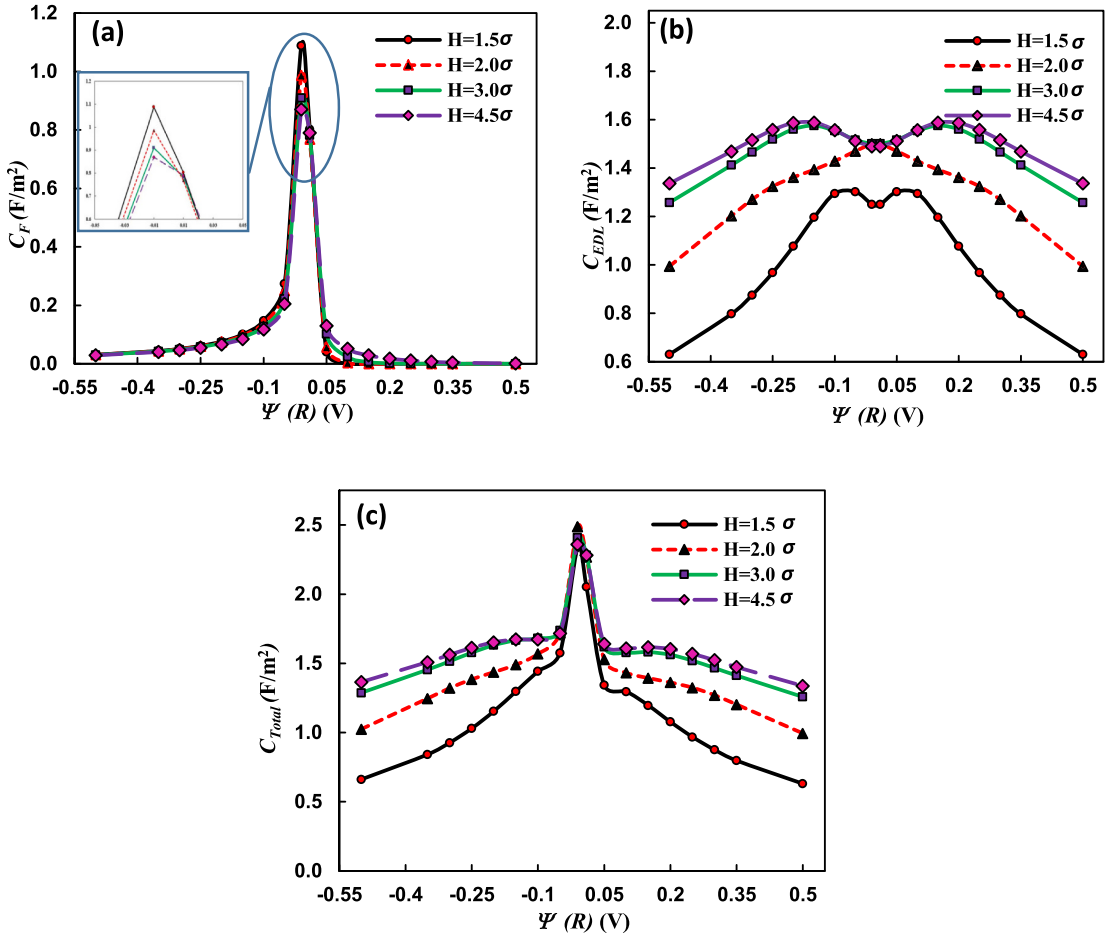

Fig. 6. The integral Faradic ***a***, EDL ***b*** and total capacitance curves ***c*** for core-shell spherical pore with $R_{in} = 2\sigma$ while the R_{out} varies, including 3.5, 4, 5, and 6.5σ at concentrations equal to 1.0 M.

condition as Fig. 6a. As one can see, the camel curves have been observed for pore thickness equals to $H = 1.5$, 3, and 4.5σ. It means a bell shape for EDL capacitance is observed for the case of $H = 2\sigma$. This may be explained via the fact that only for this pore size a typical two order layer of ions may be formed into the pore, one adjacent to the convex surface and the other next to the concave surface. Both of them are compact even at such a low potential. Our mean is for smaller sizes, $H < 2\sigma$, if the two layers form, they should be disorderly necessarily. Also, for larger sizes multiple diffuse layers may be formed leading to a camel curve. This unique layer ordering, is only related to the pore size equal to $H = 2\sigma$. since for such a case each of the layers is formed in contact with the wall, and therefore the effect of the wall on their ordering is maximum. In fact, for a 1.0 M concentration, where the diffuse layer is formed, other sizes, the wall effect on the formation of a compact layer for $H = 2\sigma$, is remarkable, which leads to a bell-shaped capacitance curve.

In Fig. 6c, the total capacitance curves for various pore sizes have been shown. The total capacitance at the whole range of the potential

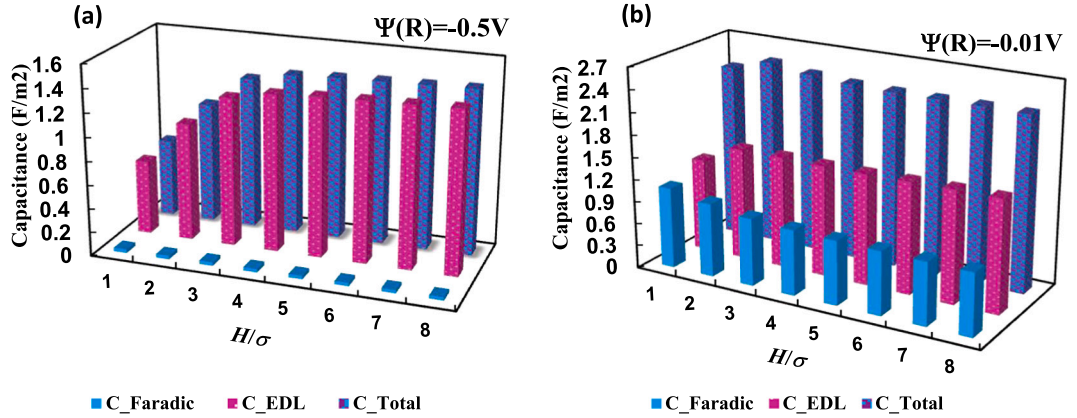

Fig. 7. Column graph for the total capacitance and its contribution related to Faradic and EDL ones for pores with the core-shell model at ***a*** − 0.5 V and ***b*** − 0.01 V potential for 1.0 M concentration.

(negative or positive) range, except near zero, increases as the pore size increases. Which is attributed to the increases of EDL capacitance with size. But at nearly zero potential, where the capacitance behavior is determined by both EDL and Faradic capacitance, a systematic behavior with size is not observed.

To investigate the behavior of total capacitance with size more precisely at different potentials, we have plotted Figs. 7. Fig. 7a and b, show the total, EDL and Faradic capacitances versus pore size at two potentials equal to −0.5 V and − 0.01 V respectively under the same conditions as Fig. 6a. As it is clear from, Fig. 7a the total capacitance mainly determined by its EDL contributions. But, the role of Faradic capacitance is significant at $\Psi(R) = -0.5$ V (see Fig. 7b).

3.3. EDL thickness and capacitance behavior

As we know, the microscopic structure of the EDL, the amount of the charge into the pore, and therefore the total capacitance has a close relation with the behavior of the MEP and may be interpreted via the potential drop on the Stern region, where this region is free of ions. Our meaning from the potential drop in the Stern region, according to the modeling of ions as a hard charge sphere, refers to the potential difference between the surface potential, $\Psi(R)$, and the potential at $R_{out} - \frac{\sigma}{2}$ or the zeta potential.

Both the behaviors of the total capacitance and potential drop in the Stern region versus size have been plotted in Fig. 8a and b, respectively, for different concentrations, including 0.5, 1.0, and 2.0 M at $\Psi(R) = -0.5$ V.

As shown in the figure, the total capacitance for small pores does not remarkably change with concentration, while for larger pore size it increases with concentration. For a fixed concentration, the capacity at first increases significantly with pore size but its variation with size becomes slower for higher pore size. To interpret this behavior we investigate the potential drop in the Stern region, which we have demonstrated in our previous work that is closely related to the structure of EDL within the pores [38]. According to our model, the Stern region near the outer sphere is defined as the interval between R_{out} and $R_{out} - \frac{\sigma}{2}$. Therefore, the value of the potential drop in the Stern region, $|\Psi(R_{out}) - \zeta|$, where ζ, is the zeta potential, according to Eq. (17) is;

$$\Psi(R_{out}) - \zeta = \left(\frac{1}{R_{out}} - \frac{1}{R_{out} - \left(\frac{\sigma}{2}\right)}\right)\left(\frac{q_1 + q_{ion}}{\varepsilon}\right) \tag{21}$$

According to Fig. 8b, for all examined concentrations, $|\Psi(R) - \zeta|$ versus pore size has a same behavior with those ones for the total capacitance with size. Similar to our previous work [38], we may say that small value of the potential drop, points to the formation of a wide diffuse layer which leads to remarkable EDLs overlap into the pore. In fact, for small pores, where the distance between the two convex and concave surfaces is small, the formed EDLs two surfaces overlap to each other which causes a smaller value for total capacitance. Also, for such small pore sizes increasing the concentration does not have a remarkable effect on the potential drop and therefore the total capacitance. It means increasing the concentration can have no remarkable effect on counterion adsorption because of the small pore size. Conversely, when the pore size increases, the value of potential drop increases, leading to a formation of a thinner diffuse layer, lower EDL overlap, and therefore an increase in capacitance (see Fig. 8a and b).

In fact, increasing the concentration for large enough pores leads to a greater adsorption of counter ions, and therefore a thinner diffuse layer leads to a more potential drop and therefore higher values for total capacitance.

Such a study has been done at lower potentials. Fig. 9a shows the behavior of total capacitance versus pore size at an applied potential equal to −0.01 V for different electrolyte concentrations, including 0.5, 1.0, and 2.0 M. In this case, R_{in} has been fixed at 2σ, while R_{out} varies from 3.5 to 10σ. In fact, for this study, the effect of the amount of curvature of the concave wall is investigated. This figure shows that at low and moderate concentrations, total capacitance initially increases with pore size, then remains approximately constant for larger sizes at 1.0 M. The maximum appeared in the plot related to is due to $H = 2\sigma$. This is due to the formation of two compact layers inside the pore as we discussed in Fig. 5a. At 2.0 M concentrations, the capacitance trend with pore size changes: it decreases with size and then remains constant for larger sizes.

In Fig. 9b, the behavior of the potential drop in the Stern region is depicted as the pore size increases under the same conditions as in Fig. 9a.

Again, the behavior of the potential drop is so similar to these ones for the total capacitance. Considering the low applied potential, the lowest potential drop has been observed at low and moderate concentrations for small pores. At this condition the EDL thickness is wide, due to the low electrode potential and also smaller concentration which leads to a decrease in total capacitance. As seen in Fig. 9b, at low and moderate concentrations, the potential drop increases with the pore size up to a certain radius, after which it remains relatively constant. An increase in the potential drop for larger pores suggests the development of a thin diffuse layer within the pore, which is significantly influenced by the concentration and applied potential. This figure. Also shows at a moderate concentration,1.0 M, for a pore with a thickness equal to 2σ,

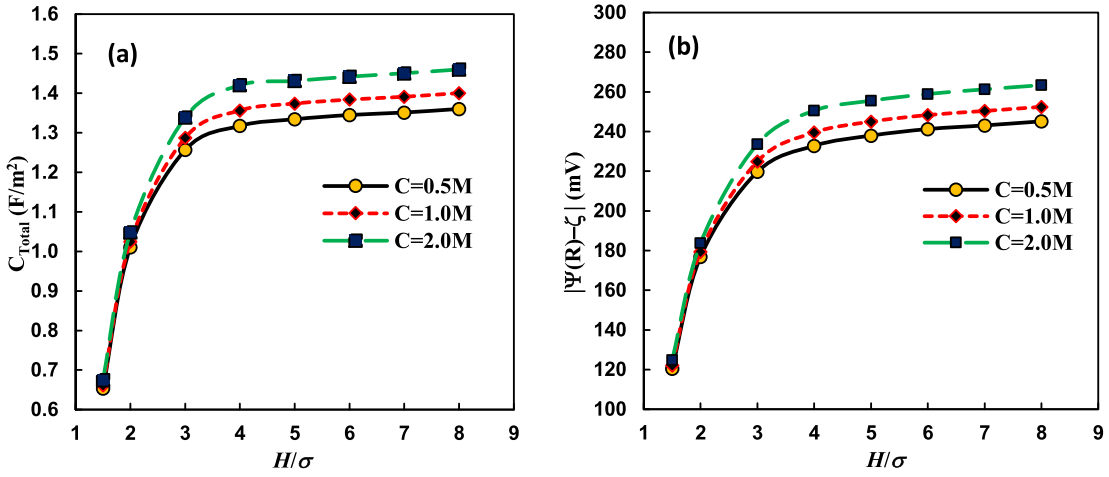

Fig. 8. ***a*** The total capacitance and ***b*** Behavior of $|\Psi(R) - \zeta|$ as a function of pore size for different concentrations of electrolyte equal to 0.5, 1.0, and 2.0 M and applied potential equal to −0.5 V.

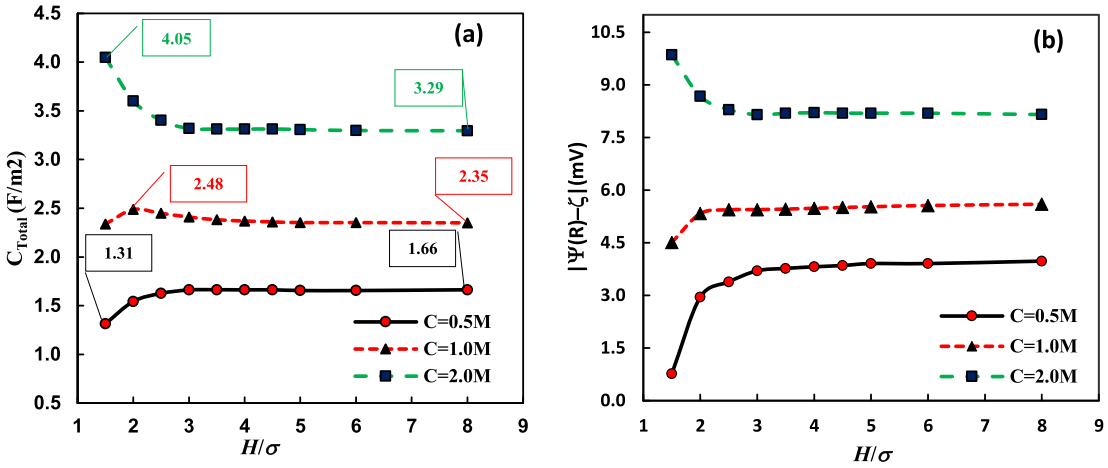

Fig. 9. ***a*** The total capacitance and ***b*** behavior of $|\Psi(R) - \zeta|$ as a function of pore size for different concentrations of HCl equal to 0.5, 1, and 2 M and applied potential equal to −0.01 V.

the potential drop for that has the highest value while leading to a greater capacitance. For this size, a thinner diffuse layer is formed, and therefore less overlap happens. As the concentration rises to 2 M, the maximum potential drop is related to the smaller pore, while an increase in pore size results a decrease in the potential drop.

In general, the concentration factor at low applied potential, plays a key role in determining the thickness of EDL and can influence the potential drop in the Stern region.

Such a study has been done for spherical shell with $R_{out} = 10\sigma$, while we alter the radius of the spherical core from 2 to 8.5 σ. On other words, the investigation involved a change in the amount of the curvature of the convex surface and its impact on the total capacitance is studied. The result of such a study is shown in the supporting information (Fig. S1a), which shows the total capacitance versus pore size as the radius of the convex wall increases at an applied potential equal to −0.01 V. The electrolyte concentrations have different values, including 0.5, 1.0, and 2.0 M.

As we have shown the total capacitance increases with H for both concentrations equal to 0.5 and 1.0 M. In fact, increasing convex surface curvature (decreased R_{in}) increases capacitance. As R_{in} decreases further, the change in capacitance with pore size becomes smoother. It is clear that a spherical pore thickness may be generated by different values of R_{in} and R_{out}, our result shows that if a space value of H degenerated by more value of Rin and therefore larger value of ($R_{out} = R_{in} + H$) leads to more values of capacitance.

Fig. S1b in the Supporting information illustrates the behavior of the potential drop versus H under the same conditions as Fig. S1a. As one can see, the behavior of the in potential drop with size is correlated with the behavior of the capacitance with size.

3.4. *Why the core-shell geometry is suggested for the porous electrodes?*

We have compared the amount of total capacitance for various spherical geometries in this section. To do so, we have selected three systems with spherical symmetries: a core-shell spherical pore with $R_{in} = 2\sigma$ and $R_{out} = 3.5\sigma$, a shell or charged spherical pore with $R_{shell} = 3.5\sigma$, and a nanoparticle or charged spherical core with $R_{core} = 2\sigma$, as shown in Fig. 10a. It is important to note that in this investigation, we separated the effects of the convex surface from the concave one in the case of the shell and core, respectively. While the effects of both convex and concave surfaces come into account in the case of the core-shell model. Where we also assume that the same density functional groups, the applied potential on their surfaces, and all other electrolyte parameters are the same. As we have expressed in the previous section, the concentration of H^+ inside the pore strongly influences the extent of electrochemical reactions on the electrode surface and therefore the Faradic capacitance. Since the density distributions around the convex and concave walls are different, therefore the reactivity and also the Faradic capacitance related to them are different.

Fig. 11a shows the average densities of H^+ versus Ψ (R) for the core and shell, as well as the spherical core-shell, when the other conditions are the same as in Fig. 3a. The average density of H^+ around the spherical core was calculated using Eq. (22), while Eq. (23) was used for the spherical shell.

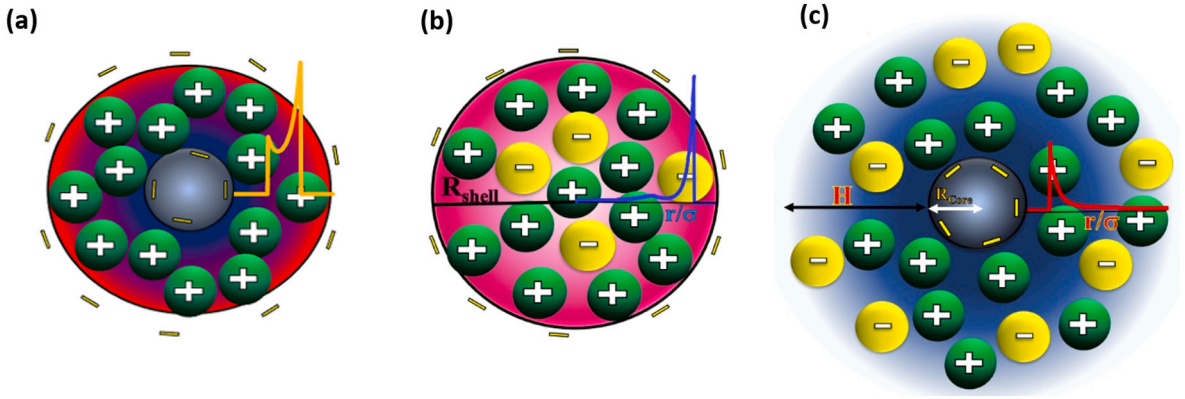

Fig. 10. Schematic presentation of core-shell model with ions inside it ***a***, whereas the core and shell are presented in ***b*** and ***c***.

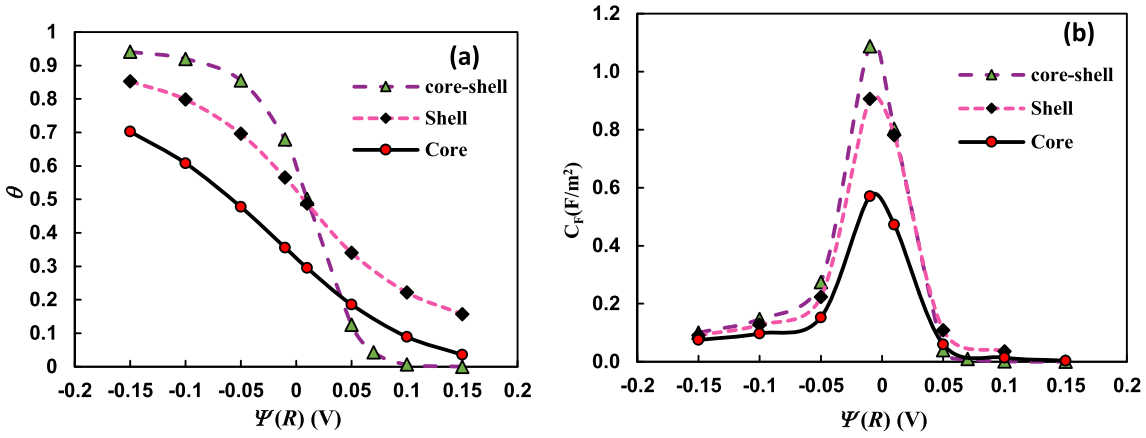

Fig. 11. The effect of different geometries on ***a*** average density of H^+ ions, ***b*** reactivity of functional group, and ***c*** Faradic capacitance as a functional potential at concentration equal to 1.0 M. The radius of spherical pore is 2σ, spherical shell has radius equal to 3.5σ, and in the core-shell pore $R_{in} = 2\sigma$ where $R_{out} = 3.5\sigma$.

$$\overline{\rho}_{H^+Core} = \frac{4\pi}{\frac{4}{3}\pi\left[(R_{Core}^{*} + d)^3 - (R_{core}^{*})^3\right]} \int_{R_{core}^{*}}^{R_{Core}^{*}+d} \rho_{H^+}^{*}(r) r^{*2} dr^{*} \tag{22}$$

$$\overline{\rho}_{H^+shell} = \frac{4\pi}{\frac{4}{3}\pi(R_{shell}^{*})^3} \int_{0}^{R_{shell}^{*}} \rho_{H^+}^{*}(r) r^{*2} dr^{*} \tag{23}$$

where d has been selected equal to H.

As one can see in Fig. 11a, when the potential is negative, the average densities of H^+ inside the core-shell model are larger than those ones for the core and also for the shell models. This fact may be explained via the point that applying the potential on both convex and concave walls of the core-shell simultaneously creates more electric field beside more confinement effect, which leads to more adsorption of H^+ ions. This fact increases the reaction and therefore the Faradic capacitance. Also, according to our results, the average densities of H^+ around the spherical core, convex wall, are smaller than that those ones from the spherical shell, concave surface. However, when a positive potential is applied, the desorption of H^+ occurs more easily for the core-shell model.

Fig. 11b shows the functional groups' reactivity, θ, against the applied potentials for the core-shell pore, as well as the spherical shell and core ones. As depicted in this figure, the Faradic reaction occurs more within the core-shell spherical pore because of more concentration of H^+. Also, when the potential is positive, θ goes to zero at smaller positive potentials for the core-shell model which points to its easy desorption of H^+.

Fig. 11c illustrates the Faradic capacitance curves of these spherical geometries. Again, for the core-shell spherical pore, as we expected, the Faradic capacitance is more than those for the others geometries.

This investigation has been also done for other pore sizes where the results are summarized in Fig. 12a. Fig. 12a shows the maximum value of faradic capacitance, which occurs approximately around −0.01 V, versus pore size. In detail, we have compared the maximum value of the Faradic capacitance for spherical shell with core-shell models, where R_{shell} for both cases varies from 3.5 to 10σ. Note that in the case of core-shell, the size of the core has been fixed at $R_{in} = 2\sigma$ where the other conditions are similar to those ones in Fig. 11a.

As one can see, the Faradic capacitance for shell and core-shell pores exhibits a decreasing trend with pore size. It means increasing the pore size reduces the pore selectivity for H^+, allowing co-ions to adsorb along with it, which leads to decreasing the concentration of H^+ into the pore. In fact, reducing the amount concavity of the wall or increasing R_{shell} leads to smaller adsorption of H^+ for both models, which causes decrease the Faradic capacitance. Also, according to this figure the Faradic capacitance for the core-shell pore is greater than those ones for shells, especially at smaller sizes. The larger values of C_F for the case of core-shell model may be interpreted via more confinement effect in addition to the more electric field into the core-shell pore.

A similar investigation has been done for Faradic capacitance but for the other two models including core and core-shell in Fig. 12b. In this study, we selected different radius for core including $R_{core} = 3.5$, 4, 6, 6.5, 7, 8, and 8.5σ where the potential is equal to −0.01 V, which yielded

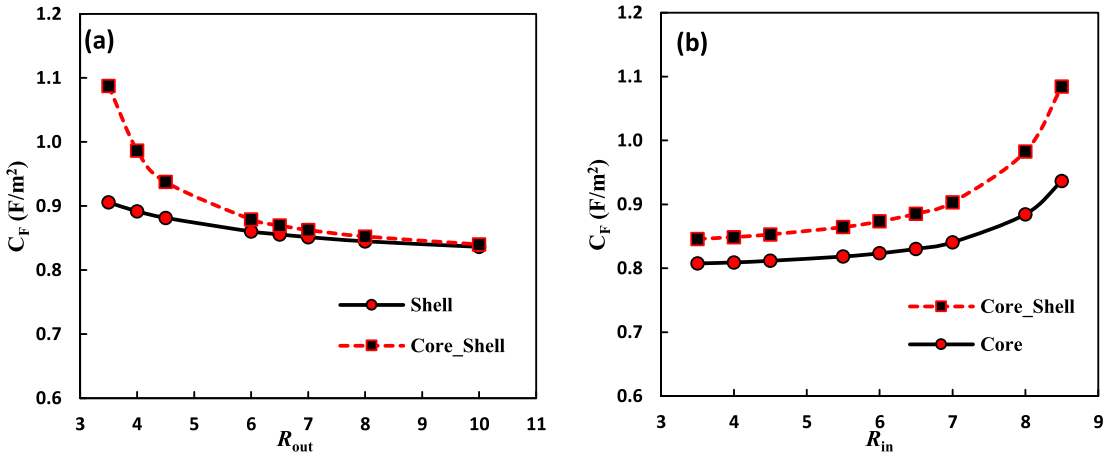

Fig. 12. A comparison of the Faradic capacitance between core-shell pores and ***a*** spherical shell with radii of 3.5, 4, 4.5,6, 6.5, 7, 8, and 10σ ***b*** spherical core with radii 3.5, 4, 4.5, 6, 6.5, 7, 8 and 8.5σ at applied potential of −0.01 V in concentration of electrolyte equal to 1.0 M.

the maximum Faradic capacitance. For the case of core-shell the value of R_{out} has been selected equal to 10σ, and the different value of R_{in} is the same as that for core geometry. In this case, to obtain the average density of H^+, using Eq. (22) we set d equal to H.

Again core-shell model has greater Faradic capacitances than those ones related to the spherical core. This is due to the confinement effects and the stronger of electric field, which lead to more absorption of H^+, thereby increasing the Faradic capacitance. The difference of the Faradic capacitance between core and core-shell model, decreases as the value of "H" increases, as R_{in} decreases, because the charged surfaces and confinement effects decrease with size. Also, the decrease in the behavior of Faradic capacitance with R_{in} may be interpreted as a decrease in the amount of the convexity of the wall with increasing R_{core} which causes more H^+ absorption.

According to the above explanation, it seems that the Faradic reaction is better done for the core-shell model in comparison to the other spherical geometries. As we explained before this is related to the more confinement effect and also more electric field in this kind of pore. To separate these two effects and also investigate another study to know which one of these two factors has a greater impact on the values of the capacitance. To do so, we have compared the result of the core-shell model with another geometry, called the yolk-shell model.

To separate the effect of the confinement effect on total capacitance from the effect of the strength of the electric field in the case of core-shell pore, we introduced another pore as yolk-shell model. The geometry of yolk-shell pore is the same as that for core- shell but in the case of core-shell model, the potential is imposed on both shell and core simultaneously, while for the yolk-shell model, the potential is only applied on the shell, leaving the core without any applied potential (see Fig. 13). In fact, in this comparison, the effect of the confinement for both types of pores is the same, while their difference is related to the electric field strength. Fig. 13a and b show a schematic presentation of the core-shell and yolk-shell model, along with the behavior of MEP. The applied potential on both pores is equal to −0.5 V. Remember this potential is applied on both surfaces of the core and the shells for the core-shell pore but only applied on the shell (no core) in the case of the yolk-shell model. The size of the spherical core (R_{in}) is equal to 2σ, while for the spherical shell (R_{out}) is 3.5σ.

The behaviors of $\Psi(r)$ in the two types of pores have been shown in Fig. 13c. As we know, the behavior of $\Psi(r)$ and also its amount at each point into the pore may be interpreted by the amount of the net ion charge, the type of the ion distributions, and the amount of the wall's potential. As one can see, $|\Psi(r)|$ in the case of yolk-shell by decreasing the distance from the shell reduces. As a result of the applied potential on both convex and concave walls of the core-shell pore, $|\Psi(r)|$ has higher values in the whole of the pore in comparison to the yolk-shell model. In fact, the strength of the electric field in the case of the core-shell is more than those ones for the yolk-shell model. Also, our investigations show that the net ion charge into the core-shell model is larger than that of the yolk-shell due to the strength of the electric field.

This result that the electric field and therefore Q_{ion} into the core-shell model are more than those one for the yolk-shell is expectable. We have obtained total capacitance, C_T, for the two types of the pore versus size at $\Psi(R) = -0.01$ V, where their differences, $C_{T(core-shell)} - C_{T(yolk-shell)}$, have been plotted in Fig. 14a. The electrolyte concentration is equal to 1.0 M, the size of the spherical core (R_{in}) is 2σ, while the size of the spherical shell (R_{out}) varied from 3.5 to 10σ.

Note that the difference between those two total capacitances is related to the strength of the electric field or the connection of the core to the potential. Another comparison between the total capacitances for the shell and the yolk-shell, $C_{T(shell)} - C_{T(yolk-shell)}$, has been done in Fig. 14a. Note that by this comparison, the role of the confinement effect is determined. This figure shows that the effect of the strength of the field is more important with respect to the confinement effect, at least at such a low potential.

Fig. 14b is the same as Fig. 14a but for $\Psi(R) = -0.5$ V. This figure shows that the effect of the electric field strength is not so important for small sizes, but for larger sizes it has a main role in capacitance. By comparison of Fig. 14a and b we may say that the confinement effect only at low potential for smaller pore size has effect on increases the capacitance. But at higher potential, for very small sizes, the confinement has a reversed effect because of the limited space; it decreases the capacitance, and on the other words, the shell model is superior.

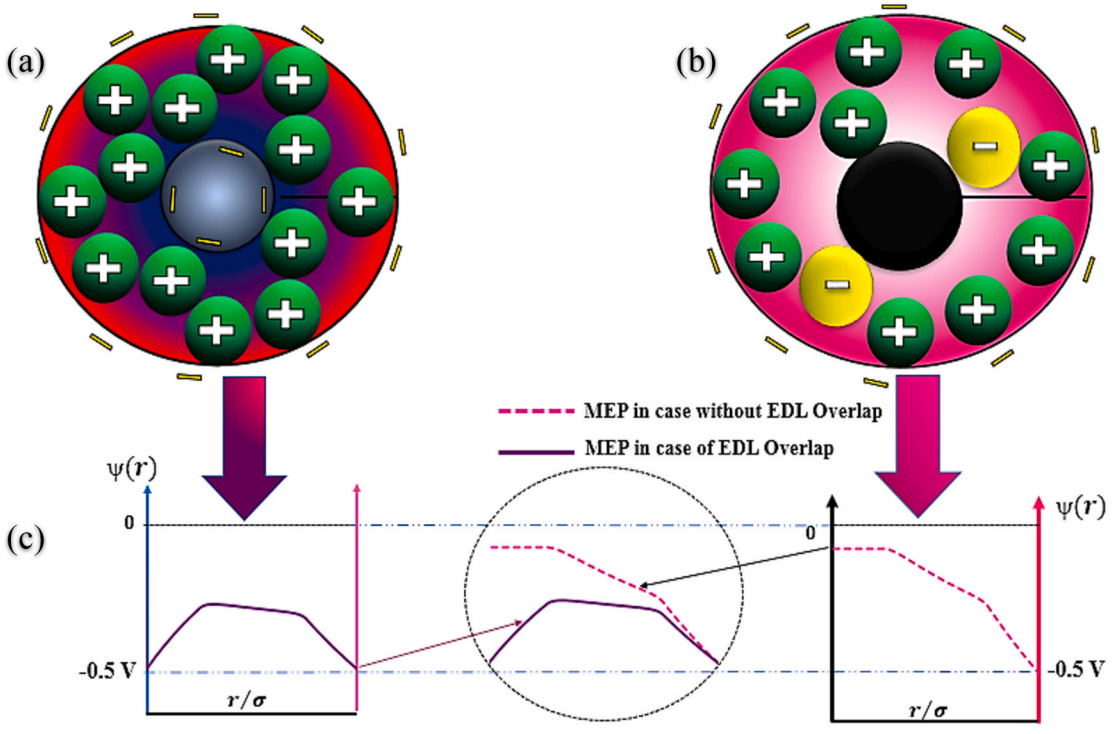

Fig. 13. ***a*** core-shell model, ***b*** yolk-shell model and ***c*** the mean electric potential inside the core-shell and yolk-shell pores.

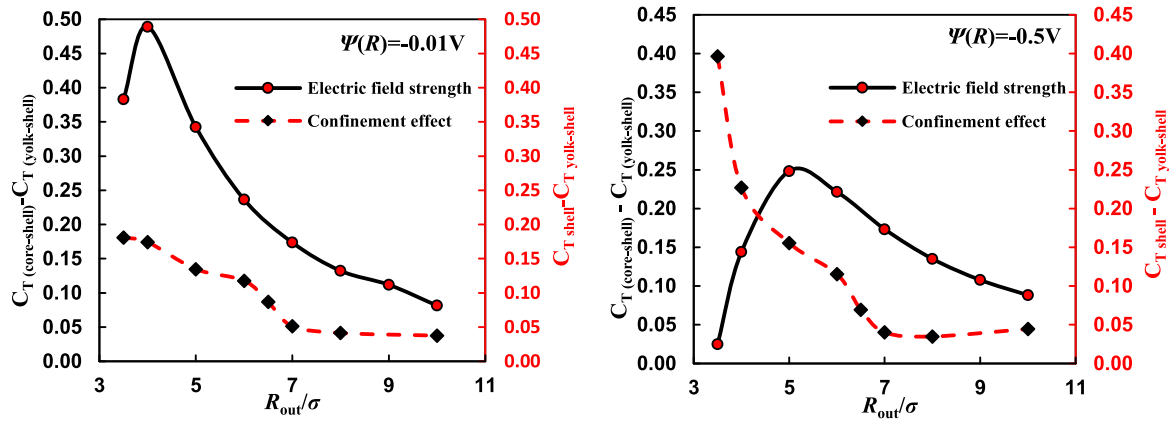

Fig. 14. A separated of the confinement effect from strength of the electric field at low potential ***a*** – 0.01 V and high potential ***b*** – 0.5 V. A comparison between the total capacitance of the core-shell from yolk-shell, strength of the electric field, and between the total capacitance for the shell and the yolk-shell, the confinement effect.

Since we previously noted that spherical geometries such as hollow metal oxides, including yolk-shell, core, shell, and multi-shell configurations are experimentally realizable, it is instructive to related our theoretical results to relevant experimental observations [39].

In particular, study on nanoporous $CuCo_2O_4$ double shelled hollow microspheres have shown that these structures exhibit higher capacitance than core or shell structures alone due to their large surface area and low density, which is good agreement with our results [39]. In fact, the core-shell model in that study is somewhat similar to the yolk-shell model in our study, where the potential is applied to the shell, increasing the capacitance compared to cases using only the core.

In this study, the core-shell models are mainly considered with the potential applied to both surfaces. Consequently, in our computational results, core-shell structures exhibit higher capacitance than the yolk-shell, core, or shell models owing to the potential applied to both the core and shell. A comprehensive comparison of all four spherical configuration has been presented in the supporting information (Fig. S2), which shows the summarized differences in capacitance behavior for examined geometries.

4. Conclusions

This study investigates the effects of concave and convex curvatures in core-shell pores on EDL and Faradic capacitances using theoretical methods and electrochemical reaction. The results show that increasing electrolyte concentration increases both Faradic and EDL capacitances. Also, the EDL capacitance curve shows a transitioning from a camel shape to a bell shape depending on concentration and pore size. The total capacitance curve exhibits a bird shape at low concentrations and a bell shape at high concentrations. Studies on pore size show that increasing pore size decreases Faradic capacitance, but EDL capacitance behaves differently at low and high potentials. In the core-shell model with thickness H=2σ, only at 1.0 M does the capacitance curve take on a bell shape, indicating the formation of compact ionic layers. Leading to maximum EDL capacitance at nearly zero potential. In fact, for this pore size, the two layers are in contact with the pore walls and are more ordered.

The potential drop in the Stern region was also considered. Our results showed that at low potential, increasing electrolyte concentration leads to a thinner diffuse layer, causing an increase in capacitance. At high potential and small pore sizes, EDL overlap decreases the total capacitance. For larger pores, the potential drop increases, leading to a thinner diffuse layer and hence higher capacitance.

Compared to other geometries, the core-shell model shows higher Faradic capacitance due to stronger electric field effects and spatial confinement.

The yolk-shell model was introduced to separate the effects of confinement and electric field strength. Comparing the effects of electric field strength and confinement, we found that at low potential, the electric field strength is more important for all pore sizes, while at high potentials, it mainly affects larger pore sizes.

CRediT authorship contribution statement

Ezat Keshavarzi: Writing – review & editing, Validation, Supervision, Project administration, Funding acquisition, Formal analysis, Conceptualization. **Fatemeh Dehghan Safiabad:** Writing – original draft, Visualization, Resources, Investigation, Data curation, Conceptualization. **Samaneh Safdaar:** Software, Resources, Methodology, Investigation, Conceptualization.

Author statement

The authors confirm that this manuscript is original, has not been published previously, and is not under consideration elsewhere. All authors have contributed to the work, have read and approved the final version of the manuscript, and declare no conflict of interest.

Declaration of competing interest

The authors whose names are listed immediately below certify that they have NO competing financial interests or personal relationships that could have appeared to influence the work reported in this paper.

Acknowledgments

The authors would like to acknowledge the Isfahan University of Technology Research Council for their financial support.

Appendix A. Supplementary data

Supplementary data to this article can be found online at https://doi.org/10.1016/j.est.2026.122209.

Data availability

Data will be made available on request.

References

[1] C. Qiu, L. Jiang, Y. Gao, L. Sheng, Effects of oxygen-containing functional groups on carbon materials in supercapacitors: a review, Mater. Des. 230 (2023) 111952.

[2] K.K. Kar, Handbook of Nanocomposite Supercapacitor Materials II, Springer, 2020.
[3] P. Simon, Y. Gogotsi, Materials for electrochemical capacitors, Nat. Mater. 7 (2008) 845–854.
[4] Y. Wang, Y. Song, Y. Xia, Electrochemical capacitors: mechanism, materials, systems, characterization and applications, Chem. Soc. Rev. 45 (2016) 5925–5950.
[5] S. Banerjee, B. Mordina, P. Sinha, K.K. Kar, Recent advancement of supercapacitors: a current era of supercapacitor devices through the development of electrical double layer, pseudo and their hybrid supercapacitor electrodes, J. Energy Storage 108 (2025) 115075.
[6] H. Ji, X. Zhao, Z. Qiao, J. Jung, Y. Zhu, Y. Lu, L.L. Zhang, A.H. MacDonald, R. S. Ruoff, Capacitance of carbon-based electrical double-layer capacitors, Nat. Commun. 5 (2014) 3317.
[7] H. Tao, C. Lian, H. Liu, Multiscale modeling of electrolytes in porous electrode: from equilibrium structure to non-equilibrium transport, Green Energy Environ. 5 (2020) 303–321.
[8] H. Shen, Y. Zhu, I. Zada, H. Li, S.W. Bokhari, S. Zhu, Y. Li, Investigation of strategies for improving the energy density of symmetric electrical double-layer capacitors, J. Energy Storage 79 (2024) 110127.
[9] B. Yan, J. Zheng, L. Feng, Q. Zhang, C. Zhang, Y. Ding, J. Han, S. Jiang, S. He, Pore engineering: structure-capacitance correlations for biomass-derived porous carbon materials, Mater. Des. 229 (2023) 111904.
[10] C. Largeot, C. Portet, J. Chmiola, P.-L. Taberna, Y. Gogotsi, P. Simon, Relation between the ion size and pore size for an electric double-layer capacitor, J. Am. Chem. Soc. 130 (2008) 2730–2731.
[11] M. Jiménez, S. Ahualli, P. Arenas-Guerrero, M. Fernández, G. Iglesias, A. Delgado, Multiionic effects on the capacitance of porous electrodes, Phys. Chem. Chem. Phys. 20 (2018) 5012–5020.
[12] M.L. Jiménez, S. Ahualli, M.M. Fernández, The Electrical Double Layer as a Capacitor. Evaluation of Capacitance in Different Solutions: Effect of Ion Concentrations, Sizes, and Valencies, in: Interface Science and Technology, Elsevier, 2018, pp. 39–62.
[13] H. Wang, R. Fan, J. Miao, J. Deng, Y. Wang, Oxygen groups immobilized on micropores for enhancing the pseudocapacitance, ACS Sustainable Chem. 7 (2019) 11407–11414.
[14] H. Wang, Y. Shao, S. Mei, Y. Lu, M. Zhang, J.-k. Sun, K. Matyjaszewski, M. Antonietti, J. Yuan, Polymer-derived heteroatom-doped porous carbon materials, Chem. Rev. 120 (2020) 9363–9419.
[15] J. Yang, A. Gallegos, C. Lian, S. Deng, H. Liu, J. Wu, Curvature effects on electric-double-layer capacitance, Chin. J. Chem. Eng. 31 (2021) 145–152.
[16] B. Peng, Y.-X. Yu, Ion distributions, exclusion coefficients, and separation factors of electrolytes in a charged cylindrical nanopore: a partially perturbative density functional theory study, J. Chem. Phys. 131 (2009).
[17] K. Yan-Shuang, W. Hai-Jun, Density functional theory approach for charged hard sphere fluids confined in spherical micro-cavity, Chin. Phys. Lett. 26 (2009) 126102.
[18] Y.-X. Yu, J. Wu, G.-H. Gao, Density-functional theory of spherical electric double layers and ζ potentials of colloidal particles in restricted-primitive-model electrolyte solutions, J. Chem. Phys. 120 (2004) 7223–7233.
[19] J. Seebeck, C. Merlet, R.H. Meißner, Elucidating curvature-capacitance relationships in carbon-based supercapacitors, Phys. Rev. Lett. 128 (2022) 086001.
[20] A. Reindl, M. Bier, S. Dietrich, Electrolyte solutions at curved electrodes. I. Mesoscopic approach, J. Chem. Phys. 146 (2017).
[21] Y. Chen, X. Zhang, D. Zhang, P. Yu, Y. Ma, High performance supercapacitors based on reduced graphene oxide in aqueous and ionic liquid electrolytes, Carbon 49 (2011) 573–580.
[22] M. Jerigová, M. Odziomek, N. López-Salas, "We are Here!" oxygen functional groups in carbons for electrochemical applications, ACS Omega 7 (2022) 11544–11554.
[23] Y. Chen, Z. Zhang, Z. Huang, H. Zhang, Effects of oxygen-containing functional groups on the supercapacitor performance of incompletely reduced graphene oxides, Int. J. Hydrog. Energy 42 (2017) 7186–7194.
[24] Y.J. Oh, J.J. Yoo, Y.I. Kim, J.K. Yoon, H.N. Yoon, J.-H. Kim, S.B. Park, Oxygen functional groups and electrochemical capacitive behavior of incompletely reduced graphene oxides as a thin-film electrode of supercapacitor, Electrochim. Acta 116 (2014) 118–128.
[25] H. Su, C. Lian, A. Gallegos, S. Deng, Y. Shang, H. Liu, J. Wu, Microscopic insights into the faradaic reaction effects on the electric double layers, Chem. Eng. Sci. 215 (2020) 115452.
[26] Y.-A. Chen, Y.-T. Wang, H.S. Moon, K. Yong, Y.-J. Hsu, Yolk–shell nanostructures: synthesis, photocatalysis and interfacial charge dynamics, RSC Adv. 11 (2021) 12288–12305.
[27] Y.J. Hong, J.-K. Lee, Y.C. Kang, Yolk–shell carbon microspheres with controlled yolk and void volumes and shell thickness and their application as a cathode material for Li–S batteries, J. Mater. Chem. A 5 (2017) 988–995.
[28] H. Ren, R. Yu, Hollow multi-shelled structures for energy conversion and storage applications, Inorg. Chem. Front. 6 (2019) 2239–2259.
[29] M. Zhu, J. Tang, W. Wei, S. Li, Recent progress in the syntheses and applications of multishelled hollow nanostructures, Mater. Chem. Front. 4 (2020) 1105–1149.
[30] Y. Rosenfeld, Free-energy model for the inhomogeneous hard-sphere fluid mixture and density-functional theory of freezing, Phys. Rev. Lett. 63 (1989) 980.
[31] Y.-X. Yu, J. Wu, Structures of hard-sphere fluids from a modified fundamental-measure theory, J. Chem. Phys. 117 (2002) 10156–10164.
[32] Z. Tang, L. Mier-y-Teran, H. Davis, L. Scriven, H. White, Non-local free-energy density-functional theory applied to the electrical double layer: part I: symmetrical electrolytes, Mol. Phys. 71 (1990) 369–392.
[33] A. Helmi, E. Keshavarzi, The role of concavo-convex walls of a nanopore on the density profile, adsorption, solvation force, and capillary condensation of confined fluids: a DFT study, Chem. Phys. 433 (2014) 67–75.
[34] G. Mansoori, N.F. Carnahan, K. Starling, T. Leland Jr., Equilibrium thermodynamic properties of the mixture of hard spheres, J. Chem. Phys. 54 (1971) 1523–1525.
[35] E. Waisman, J.L. Lebowitz, Mean spherical model integral equation for charged hard spheres. II. Results, J. Chem. Phys. 56 (1972) 3093–3099.
[36] E. Keshavarzi, M. Abareghi, The effect of electro-neutrality violation inside a charged spherical cavity on the capacitance curve shape in DFT approach and interpretation of mean electrostatic potential, J. Mol. Liq. 318 (2020) 114271.
[37] S. Safdaar, E. Keshavarzi, Analytical expression for Poisson's equation in relation to a bispherical pore and examination of influence of the pore wall's concave and convex structure on the EDL capacitance curve, J. Mol. Liq. 427 (2025) 127365.
[38] E. Keshavarzi, F. Dehghan Safiabad, Surface charge regulation on the Concave Wall of a spherical silica pore, impact of the EDL overlap, potential drop in the stern region, and deviation from the Electroneutrality principle, J. Phys. Chem. C 128 (2024) 9256–9269.
[39] S.K. Kaverlavani, S.E. Moosavifard, A. Bakouei, Self-templated synthesis of uniform nanoporous $CuCo_2O_4$ double-shelled hollow microspheres for high-performance asymmetric supercapacitors, Chem. Commun. 53 (2017) 1052–1055.